Performance Analysis of XL-MIMO-OFDM Systems for High-Speed Train Communications

Qiuhao Liu, Yonghao Lin, Jiakang Zheng, Zhe Wang, Jiayi Zhang, Bo Ai

2023 IEEE International Conference on Communications Workshops (ICC Workshops) | 979-8-3503-3307-7/23/$31.00 ©2023 IEEE | DOI: 10.1109/ICCWORKSHOPS57953.2023.10283701

***Abstract*—Extremely large-scale multiple-input multiple-output (XL-MIMO) has been deemed a breakthrough technology that holds significant potential for next-generation communication. Applying XL-MIMO to high-speed train (HST) communications improves network capacity and transmission quality, overcoming the limitations of traditional technology. In this paper, we analyze the performance of XL-MIMO systems using extremely large aperture arrays (ELAAs) in line-of-sight (LoS) scenarios and investigate the factors that affect spectral efficiency (SE), including deployment modes, number of train antennas (TAs) or access points (APs), antenna area, HST position, and combining methods. We find that the minimum mean square error (MMSE) combining and large-scale fading decoding (LSFD) cooperation are crucial for HST communications. Moreover, numerical results show that increasing the number of APs enhances the average SE and decreases the distance between the APs and the rail track, leading to optimal performance. Additionally, reducing the number of TAs and antenna area can also minimize the impact of Doppler frequency offset (DFO). Furthermore, if the total number of antennas is kept constant, further improving the average SE can be achieved by decreasing the number of antennas per AP and increasing the number of APs.**

I. Introduction

Researchers are investigating the potential of communication networks beyond 5G (B5G) or 6G [1], [2]. Extremely large-scale multiple-input multiple-output (XL-MIMO) communication technology is one area of study [3]. In comparison to traditional MIMO or massive MIMO systems, XL-MIMO systems include new channel characteristics, such as a greater chance of users/scatterers not being in the far-field region because of the shrinking cell size. Additionally, railway communications utilizing XL-MIMO are of interest due to growing railway development [4]–[7]. In the propagation environment of high-speed train (HST), the line-of-sight (LoS) assumption is often possible due to the lack of scattering and reflection. The orthogonal frequency-division multiplexing (OFDM) is employed to maintain connectivity with ground cellular networks [8]. However, high mobility in railway communications can result in issues such as timing offset, phase noise, and Doppler frequency offset (DFO), causing serious inter-carrier interference (ICI) and poor performance [9]. XL-MIMO architecture provides a promising solution to tackle these challenges in high-mobility environments and making it especially suitable for HST communications.

It's important to note that most XL-MIMO research focuses on stationary environments rather than mobile scenarios. The majority of XL-MIMO studies treat each array element as sizeless and isotropic points, which may not be appropriate for extremely large aperture arrays (ELAAs) [10]. Additionally, while there has been a significant amount of research on HST communications using cell-free (CF) massive MIMO [11], [12], there has been little exploration of combining XL-MIMO with HST communications.

Our goal is to examine the potential use of XL-MIMO in HST communications and to determine the specific parameters that impact its performance. This is considered a significant contribution as it fills a gap in the current literature on XL-MIMO and its potential applications. Motivated by this, we look into how the XL-MIMO-OFDM system performs in HST communications. For uplink data transmission, we examine the adoption of minimum mean square error (MMSE) combining with local and fully centralized processing. The investigation contrasts the performance of XL-MIMO-OFDM in HST communications with cellular and small cell systems. Then, we consider an XL-MIMO-OFDM system for HST communications and results show that the use of MMSE combining and large-scale fading decoding (LSFD) cooperation in XL-MIMO-OFDM systems are necessary for HST communications and provide higher and more uniform spectral efficiency (SE) compared to cellular and small cell systems. It is interesting to find that increasing the number of APs significantly enhances the average SE and will result in a smaller distance between the APs and the railway providing the optimal point for SE. While reducing the number of train antennas (TAs) and reducing the area of the antennas can reduce the impact of DFO. Furthermore, if the total number of antennas is constant, increasing the number of APs and decreasing the number of antennas per AP will result in an improvement in average SE.

II. System Model

As shown in Fig. 1, a HST communication system using XL-MIMO-OFDM technology is considered. The system comprises K TAs spread across multiple cars of the HST and L APs organized in extremely large aperture arrays (ELAAs) along one rail trackside. Each AP has N antennas, and fronthaul links connect it to a central processing unit (CPU).

The first two authors contributed equally to this work.

This work was supported by the National Training Program of Innovation and Entrepreneurship for Undergraduates under Project 202310004138.

Q. Liu, Y. Lin, J. Zheng, Z. Wang and J. Zhang are with the School of Electronics and Information Engineering, Beijing Jiaotong University, Beijing 100044, China. (e-mail: {20211444, 20211442, jiakangzheng, zhewang_77, jiayizhang}@bjtu.edu.cn).

B. Ai is with the State Key Laboratory of Rail Traffic Control and Safety, Beijing Jiaotong University, Beijing 100044, China. (e-mail: boai @bjtu.edu.cn).

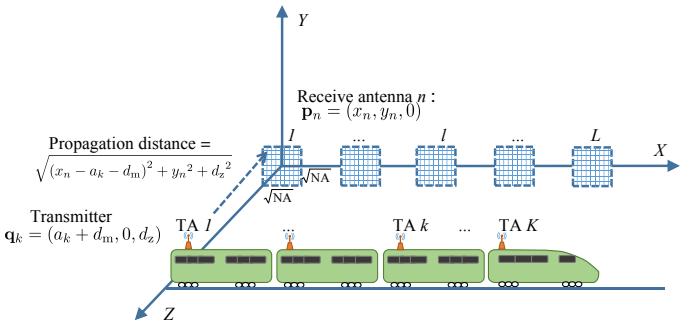

Fig. 1. HST communications with an XL-MIMO-OFDM system

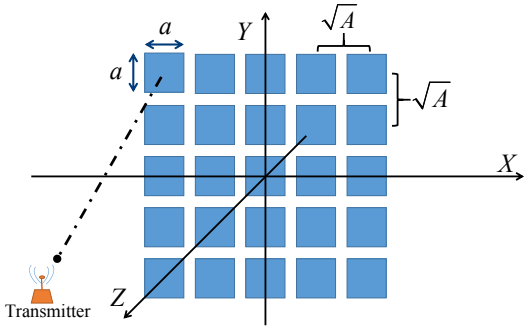

Fig. 2. A transmitter transmits to an ELAA located in the XY-plane.

All L APs are expected to serve all K TAs at the same height on the same time-frequency resource.

We assume the HST track, which is largely straight, as a straight line. To define the locations of K TAs and L APs, we employ a 3D spatial coordinate system, as displayed in Fig. 1. For $l = 1, \ldots, L$, the APs are taken to be at $\mathbf{q}_l \triangleq [a_l, 0, 0]$, with a_l being the horizontal coordinate. The distance from the rail track to the APs is denoted as d_z. For $k = 1, \ldots, K$, the TAs are located at $\mathbf{q}_k \triangleq [(a_k + d_m), 0, d_z]$, with a_k being the TA's starting abscissa position and d_m is the distance traveled by train, which represents its position. The value of d_m can be positive or negative, indicating whether the HST is moving forward or backward. The horizontal distance between TA k and AP l is computed as $d_{kl}^{ho} = a_l - (a_k + d_m)$, with the straight line distance between them being $d_{kl} = \|\mathbf{q}_l - \mathbf{q}_k\|$. The sine value of the angle of arrival (AOA) between the two points, given by the symbol φ_{kl}, is equal to $\sin(\varphi_{kl}) = d_{kl}^{ho}/d_{kl}$.

A. Channel Model

We simplify the analysis by assuming that the ELAAs, consisting of N antennas, are arranged in a planar array with a size of $\sqrt{A} \times \sqrt{A}$ for each antenna and spaced evenly on a $\sqrt{N} \times \sqrt{N}$ grid in the XY-plane. The antennas are placed edge-to-edge, yielding a total area of NA. This assumption will be used throughout the rest of the chapter, although the results are generally applicable.

The positioning and orientation of the receiving antenna in relation to the transmitter affect the effective area of the antenna. The effective area is equal to A when the antenna is oriented perpendicular to the signal direction. If not, it is decreased.

When the ELAA and transmitter are in the near field, there are three important aspects to consider for the incoming wave's amplitude and phase:

1. Variations in distance to individual antennas;
2. Different effective areas based on the angles of reception;
3. Polarization mismatch losses differ based on the angles of reception.

ELAA receives signals from an isotropic transmitter in the setup depicted in Fig. 2. The coordinates of the center of the nth receive antenna are $\mathbf{p}_n = (x_n, y_n, 0)$ if AP l is chosen to represent the ELAA's center and the antennas are numbered from left to right, top to bottom, where

$$x_n = a_l - \frac{(\sqrt{N}-1)\sqrt{A}}{2} + \sqrt{A} \bmod (n-1, \sqrt{N}),$$
$$y_n = \frac{(\sqrt{N}-1)\sqrt{A}}{2} - \sqrt{A}\left\lfloor \frac{n-1}{\sqrt{N}} \right\rfloor, \quad \text{for } n = 1, \ldots, N, \tag{1}$$

The channel between a planar receive antenna located at $\mathbf{p}_n = (x_n, y_n, 0)$ and a lossless isotropic antenna located at $\mathbf{p}_t = \mathbf{q}_k = (a_k + d_m, 0, d_z)$ can be explained as follows: The transmitter sends a signal with polarization in the Y-direction and travels in the Z-direction. The receive antenna has an area of $a \times a$ and is centered at $\mathbf{p}_n$. It is given by

$$h_n(\mathbf{p}_t) = \frac{1}{a}\int_{x_n - a/2}^{x_n + a/2}\int_{y_n - a/2}^{y_n + a/2} \epsilon(\mathbf{p}_t, \mathbf{p}_r)\, \partial x_r \partial y_r, \tag{2}$$

the integration variables are contained in $\mathbf{p}_r = (x_r, y_r, 0)$, and the impinging electric field is proportional to

$$\epsilon(\mathbf{p}_t, \mathbf{p}_r) = |\epsilon(\mathbf{p}_t, \mathbf{p}_r)|\, e^{-j\frac{2\pi}{\lambda}\|\mathbf{p}_r - \mathbf{p}_t\|}, \tag{3}$$

$$|\epsilon(\mathbf{p}_t, \mathbf{p}_r)| = \frac{\sqrt{d_z\left((x_r - a_k - d_m)^2 + {d_z}^2\right)}}{\sqrt{4\pi}\left((x_r - a_k - d_m)^2 + {y_r}^2 + {d_z}^2\right)^{\frac{5}{4}}}. \tag{4}$$

Proof: It follows from [13, Lemma 1.1] ■

The channel vector $\mathbf{h} = [h_1, \ldots, h_N]^T \in \mathbb{C}^N$ represents the flat-fading channel between the N-antenna receiver and single-antenna transmitter, where $h_n = |h_n|\, e^{-j\varphi_n}$ represents the channel from the transmitter to the nth receive antenna. The phase-shift φ_n can be calculated as

$$\varphi_n = 2\pi \cdot \bmod \left(\frac{\sqrt{\left((x_n - a_k - d_m)^2 + {y_n}^2 + {d_z}^2\right)}}{\lambda}, 1 \right). \tag{5}$$

B. Propagation Model

XL-MIMO-OFDM channel in the HST situation has ICI between neighboring subcarriers. The coherence time and

bandwidth are defined as T_c and B_c, respectively, with bandwidth B, total subcarriers M_{all}, and OFDM symbol duration T_s. Each coherence block undergoes flat-fading, with channel responses within a block being statistically identical and independent between any two blocks. To study performance, we analyze a single, statistically representative coherence block.

In the HST scenario, only the LoS path is considered, ignoring the large number of NLoS paths. Thus, the channel gain from AP l to TA k can be expressed as $\mathbf{g}_{kl} = \mathbf{h}_{kl}$, with $\mathbf{h}_{kl} \in \mathbb{C}^N$ representing the known magnitude and uniform phase of the LoS component. Then, the fading effect due to the HST's motion along the railway can then be modeled as a Rician channel with DFO.

High-speed movement leads to shorter coherence blocks and significant DFO in the HST scenario. The DFO effect may result in a decreasing correlation between the fading realizations at nearby subcarriers over time. Thus, to approximate the analysis with small errors, a full OFDM transmission can be used in a real system while only one block of it is investigated. For the analysis of a single coherence block, which has M subcarriers, we have equal channel gains, $\mathbf{g}_{il}[1] = \ldots = \mathbf{g}_{il}[M] = \mathbf{g}_{il}$, at different subcarriers. However, there is still ICI effect present.

Lemma 1. *Assuming that signals are transmitted over various subcarriers, the total signal received from all TAs at AP l can be represented in the frequency domain as*

$$\mathbf{y}_l[s] = \sum_{i=1}^{K}\sum_{m=1}^{M} \sqrt{p_i} J_{il}[m-s]\mathbf{h}_{il} x_i[m] + \mathbf{w}_l[s], \quad (6)$$

with

$$J_{il}[m-s] = \frac{\sin\left(\pi\left(m-s+\varepsilon_{il}\right)\right)}{M\sin\left(\frac{\pi}{M}\left(m-s+\varepsilon_{il}\right)\right)} e^{j\varphi_{il}}, \quad (7)$$

$$\varphi_{il} = \pi\left(1-\frac{1}{M}\right)\left(m-s+\varepsilon_{il}\right). \quad (8)$$

where $\varepsilon_{il} = \omega \sin(\varphi_{il}) = \frac{fvT_s}{c}\sin(\varphi_{il})$ is the normalized DFO between AP l and TA i. A train's velocity and the speed of light are denoted by the variables v and c, respectively, while the variable f stands for the carrier frequency.

Proof: It follows from [14, Lemma 1] ∎

III. Performance Analysis

A. XL-MIMO-OFDM with Fully Centralized Processing

When the L APs send the CPU their data signals and received pilot signals for detection and channel estimation, XL-MIMO reaches its maximum level. Put another way, all signals are sent to the CPU by the APs, which serve as relays. The following can be used to represent the signal that was received by the CPU [15]:

$$\mathbf{y}[s] = \sum_{i=1}^{K}\sum_{m=1}^{M} \sqrt{p_i}\mathbf{J}_i[m-s]\mathbf{h}_i x_i[m] + \mathbf{w}[s], \quad (9)$$

Furthermore, we have

$$\mathbf{J}_i[m-s] \triangleq \operatorname{diag}\left(J_{i1}[m-s]\mathbf{I}_N, \ldots, J_{il}[m-s]\mathbf{I}_N\right). \quad (10)$$

Using the pilot signals that were received and the channel data from the L APs, the CPU is able to calculate all MMSE channel estimates. The CPU can create an aggregated channel estimate for TA k as $\hat{\mathbf{g}}_k \triangleq \mathbf{h}_k$. The CPU then chooses a random receive combining vector $\mathbf{v}_k$ for TA k based on the sum of all individual channel estimates. The CPU receives the following signal [16], [17]:

$$\begin{aligned} y_k[s] = \mathbf{v}_k^{\mathrm{H}}[s]\mathbf{y}[s] &= \sqrt{p_k}\mathbf{v}_k^{\mathrm{H}}[s]J_k[0]\mathbf{h}_k x_k[s] \\ &+ \sum_{m\neq s}^{M}\sqrt{p_k}\mathbf{v}_k^{\mathrm{H}}[s]J_k[m-s]\mathbf{h}_k x_k[m] \\ &+ \sum_{i\neq k}^{K}\sum_{m=1}^{M}\sqrt{p_i}\mathbf{v}_k^{\mathrm{H}}[s]J_i[m-s]\mathbf{h}_i x_i[m] + \mathbf{v}_k^{\mathrm{H}}[s]\mathbf{w}[s]. \end{aligned} \quad (11)$$

Lemma 2. *The uplink SE for TA k can be achieved using the MMSE estimator $\mathrm{SE}_k^{\mathrm{fc}}[s] = \mathbb{E}\left\{\log_2\left(1+\mathrm{SINR}_k^{\mathrm{fc}}[s]\right)\right\}$ with $\mathrm{SINR}_k^{\mathrm{fc}}[s]$ is given by*

$$\begin{aligned} &p_k\left|\mathbf{v}_k^{\mathrm{H}}[s]\mathbf{q}_k[0]\right|^2 \Bigg(p_k\sum_{m\neq s}^{M}\left|\mathbf{v}_k^{\mathrm{H}}[s]\mathbf{q}_k[m-s]\right|^2 \\ &+\sum_{i\neq k}^{K}\sum_{m=1}^{M}p_i\left|\mathbf{v}_k^{\mathrm{H}}[s]\mathbf{q}_i[m-s]\right|^2 + \mathbf{v}_k^{\mathrm{H}}[s]\sigma^2\mathbf{I}_{LN}\mathbf{v}_k[s]\Big)^{-1}, \end{aligned} \quad (12)$$

where

$$\mathbf{q}_i[m-s] \triangleq J_i[m-s]\mathbf{h}_i. \quad (13)$$

Proof: The proof follows from [18, Theorem 4.1] and is thus left out. ∎

Corollary 1. *The optimal SINR for TA k can be achieved by using the MMSE combining vector $\mathbf{v}_k[s]$ and is given by*

$$p_k\left(\sum_{i=1}^{K}p_i\sum_{m=1}^{M}\mathbf{q}_i[m-s]\mathbf{q}_i^{\mathrm{H}}[m-s] + \sigma^2\mathbf{I}_{LN}\right)^{-1}\mathbf{q}_k[0], \quad (14)$$

which results in the highest performance $\mathrm{SE}_k^{\mathrm{fc,mmse}}[s] = \mathbb{E}\left\{\log_2\left(1+\mathrm{SINR}_k^{\mathrm{fc,mmse}}[s]\right)\right\}$, which $\mathrm{SINR}_k^{\mathrm{fc,mmse}}[s]$ is given as

$$\begin{aligned} &p_k\mathbf{q}_k^{\mathrm{H}}[0]\Bigg(p_k\sum_{m\neq s}^{M}\mathbf{q}_k[m-s]\mathbf{q}_k^{\mathrm{H}}[m-s] + \\ &\sum_{i\neq k}^{K}p_i\sum_{m=1}^{M}\mathbf{q}_i[m-s]\mathbf{q}_i^{\mathrm{H}}[m-s] + \sigma^2\mathbf{I}_{LN}\Big)^{-1}\mathbf{q}_k[0]. \end{aligned} \quad (15)$$

Proof: According to [18, Lemma B.10], the result in (12) follows since it's a generalized Rayleigh quotient with regard to $\mathbf{v}_k[s]$. ∎

B. XL-MIMO-OFDM with Local Processing

APs can compute local estimates of data for preprocessing, which are later sent to the CPU for decoding. The local combing vector chosen by AP l for TA k at the sth subcarrier is represented by $\mathbf{v}_{kl}[s] \in \mathbb{C}^N$. Then, based on the received signal (6), its local estimate $\check{y}_{kl}[s] = \mathbf{v}_{kl}^{\mathrm{H}}[s]\mathbf{y}_l[s]$ is acquired as [19], [20]

$$\sum_{i=1}^{K}\sum_{m=1}^{M}\sqrt{p_i}\mathbf{v}_{kl}^{\mathrm{H}}[s]J_{il}[m-s]x_i[m] + \mathbf{v}_{kl}^{\mathrm{H}}[s]\mathbf{w}_l[s]. \quad (16)$$

The combining vector with the lowest MSE is denoted as $\mathbf{v}_{kl}[s]$ and it is given by

$$p_k\left(\sum_{i=1}^{K}p_i\sum_{m=1}^{M}\mathbf{q}_{il}[m-s]\mathbf{q}_{il}^{\mathrm{H}}[m-s] + \sigma^2\mathbf{I}_N\right)^{-1}\mathbf{q}_{kl}[0], \quad (17)$$

where

$$\mathbf{q}_{il}[m-s] = J_{il}[m-s]\mathbf{h}_{il}. \quad (18)$$

The CPU combines the local estimates $\check{y}_{kl}[s]$ linearly using the LSFD weights $\alpha_{kl}[s]$ to calculate $\hat{y}_k[s] = \sum_{l=1}^{L}\alpha_{kl}^*[s]\check{y}_{kl}[s]$, which is then used for decoding $x_k[s]$. It is noted that

$$\hat{y}_k[s] = \sum_{i=1}^{K}\sum_{m=1}^{M}\sqrt{p_i}\boldsymbol{\alpha}_k^{\mathrm{H}}[s]\boldsymbol{\mu}_{ki}[m-s]x_i[m] + \mathbf{w}_k[s], \quad (19)$$

where

$$\begin{aligned}&\boldsymbol{\alpha}_k[s] \triangleq [\alpha_{k1}[s],\ldots,\alpha_{kL}[s]]^{\mathrm{T}} \in \mathbb{C}^L,\\ &\mathbf{w}_k[s] \triangleq \sum_{l=1}^{L}\alpha_{kl}^*[s]\mathbf{v}_{kl}^{\mathrm{H}}[s]\mathbf{w}_l[s],\\ &\boldsymbol{\mu}_{ki}[m-s] \triangleq \left(\mathbf{v}_{k1}^{\mathrm{H}}[s]J_{i1}[m-s]\mathbf{h}_{i1},\right.\\ &\left.\ldots,\mathbf{v}_{kL}^{\mathrm{H}}[s]J_{iL}[m-s]\mathbf{h}_{iL}\right) \in \mathbb{C}^L.\end{aligned}$$

Lemma 3. *An attainable SE of TA k is* $\mathrm{SE}_k^{\mathrm{lo}}[s] = \log_2\left(1+\mathrm{SINR}_k^{\mathrm{lo}}[s]\right)$ *with* $\mathrm{SINR}_k^{\mathrm{lo}}[s]$ *is given as*

$$\frac{p_k\left|\boldsymbol{\alpha}_k^{\mathrm{H}}[s]\mathbb{E}\left\{\boldsymbol{\mu}_{kk}[0]\right\}\right|^2}{\mathrm{Pau}_k[s] - p_k\left|\boldsymbol{\alpha}_k^{\mathrm{H}}[s]\mathbb{E}\left\{\boldsymbol{\mu}_{kk}[0]\right\}\right|^2 + \sigma^2\boldsymbol{\alpha}_k^{\mathrm{H}}[s]\ddot{\boldsymbol{\Gamma}}_k[s]\boldsymbol{\alpha}_k[s]}, \quad (20)$$

where

$$\ddot{\boldsymbol{\Gamma}}_k[s] \triangleq \mathrm{diag}\left(\mathbb{E}\left\{\|\mathbf{v}_{k1}[s]\|^2\right\},\ldots,\mathbb{E}\left\{\|\mathbf{v}_{kL}[s]\|^2\right\}\right), \quad (21)$$

$$\mathrm{Pau}_k[s] = \sum_{i=1}^{K}p_i\sum_{m=1}^{M}\mathbb{E}\left\{\left|\boldsymbol{\alpha}_k^{\mathrm{H}}[s]\boldsymbol{\mu}_{ki}[m-s]\right|^2\right\}. \quad (22)$$

Corollary 2. *The maximum effective SINR for TA k is obtained by*

$$\boldsymbol{\alpha}_k[s] = \mathbb{E}\left\{\boldsymbol{\mu}_{kk}[0]\right\}\left(\sum_{i=1}^{K}p_i\sum_{m=1}^{M}\mathbb{E}\left\{\boldsymbol{\mu}_{ki}[m-s]\boldsymbol{\mu}_{ki}^{\mathrm{H}}[m-s]\right\} + \sigma^2\ddot{\boldsymbol{\Gamma}}_k[s]\right)^{-1}, \quad (23)$$

which results in the highest value

$$\begin{aligned}\mathrm{SE}_k^{\mathrm{lsfd}}[s] = \log_2\big(1 + p_k\mathbb{E}\left\{\boldsymbol{\mu}_{kk}^{\mathrm{H}}[0]\right\}\\ \left(\sum_{i=1}^{K}p_i\sum_{m=1}^{M}\mathbb{E}\left\{\boldsymbol{\mu}_{ki}[m-s]\boldsymbol{\mu}_{ki}^{\mathrm{H}}[m-s]\right\} + \sigma^2\ddot{\boldsymbol{\Gamma}}_k[s]\right.\\ \left.-p_k\mathbb{E}\left\{\boldsymbol{\mu}_{kk}[0]\right\}\mathbb{E}\left\{\boldsymbol{\mu}_{kk}^{\mathrm{H}}[0]\right\}\right)^{-1}\mathbb{E}\left\{\boldsymbol{\mu}_{kk}[0]\right\}\Big).\end{aligned} \quad (24)$$

Proof: Similar to Corollary 1, the vector $\boldsymbol{\alpha}_k[s]$ that maximizes SINR can be calculated by using the structure of (20). ∎

C. Small Cell Systems with OFDM

In this section, a comparison is made between the systems being studied and a small cell system consisting of K TAs and L APs, where the location remains unchanged but each TA is served by a single AP, leading to optimal SE. The incoming signal is then modified by a vector calculated from the channel estimation, which is used to identify the target signal.

Theorem 1. *Then the capacity of TA k can be lower bounded by*

$$\mathrm{SE}_k^{\mathrm{sc}}[s] = \max_{l\in\{1,\ldots,L\}}\mathbb{E}\left\{\log_2\left(1+\mathrm{SINR}_{kl}^{\mathrm{sc}}[s]\right)\right\}, \quad (25)$$

where $\mathrm{SINR}_{kl}^{\mathrm{sc}}[s]$ *is given as*

$$\begin{aligned}p_k\left|\mathbf{v}_{kl}^{\mathrm{H}}[s]\mathbf{q}_{kl}[0]\right|^2\left(p_k\sum_{m\neq s}^{M}\left|\mathbf{v}_{kl}^{\mathrm{H}}[s]\mathbf{q}_{kl}[m-s]\right|^2\right.\\ \left.+\sum_{i\neq k}^{K}p_i\sum_{m=1}^{M}\left|\mathbf{v}_{kl}^{\mathrm{H}}[s]\mathbf{q}_{il}[m-s]\right|^2 + \mathbf{v}_{kl}^{\mathrm{H}}[s]\sigma^2\mathbf{I}_N\mathbf{v}_{kl}[s]\right)^{-1}.\end{aligned} \quad (26)$$

Proof: Steps similar to Lemma 2 are followed. ∎

It is important to note that the largest value in (26) is obtained by the MMSE combining from (17) and is given as

$$\begin{aligned}\mathrm{SINR}_{kl}^{\mathrm{sc,mmse}}[s] = p_k\mathbf{q}_{kl}^{\mathrm{H}}[0]\left(p_k\sum_{m\neq s}^{M}\mathbf{q}_{kl}[m-s]\mathbf{q}_{kl}^{\mathrm{H}}[m-s]\right.\\ \left.+\sum_{i\neq k}^{K}p_i\sum_{m=1}^{M}\mathbf{q}_{il}[m-s]\mathbf{q}_{il}^{\mathrm{H}}[m-s] + \sigma^2\mathbf{I}_N\right)^{-1}\mathbf{q}_{kl}[0].\end{aligned} \quad (27)$$

D. Cellular Systems with OFDM

In this scenario, we examine a cellular network with a single cell and all LN antennas at the cellular base station (BS). This resembles a specific instance of the previously discussed case, where $L = 1$ and N represents the overall number of antennas. Modeled as $\mathbf{g}_k^{\mathrm{c}} = \mathbf{h}_k^{\mathrm{c}}$, is the channel between the TA k and BS, where $\mathbf{h}_k^{\mathrm{c}} \in \mathbb{C}^{LN}$ is the LoS component.

Theorem 2. *The SE of TA k is thus given as*

$$\mathrm{SE}_k^{c}[s] = \mathbb{E}\left\{\log_2\left(1+\mathrm{SINR}_k^{\mathrm{c}}[s]\right)\right\}, \quad (28)$$

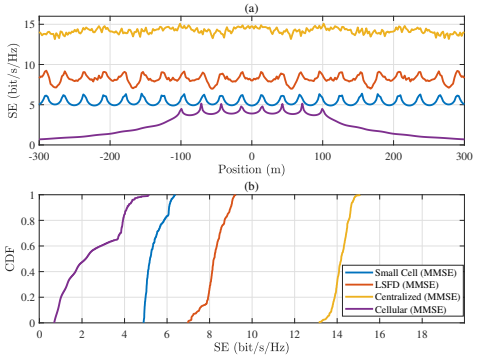

Fig. 3. (a) Comparison of SE based on the HST position using MMSE combining, small cell, and cellular scenarios. (b) CDF of SE for HST position using MMSE combining in the CF, small cell, and cellular scenarios ($K = 8, L = 10, N = 64, d_z = 50$ m, $v = 300$ km/h).

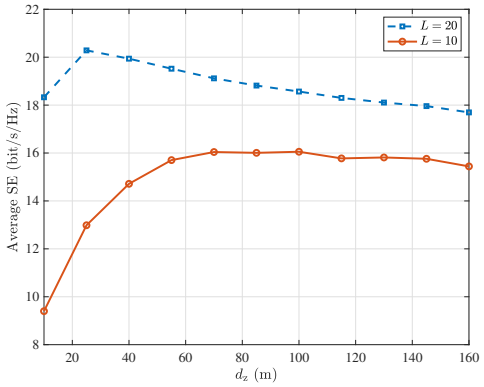

Fig. 4. Average SE in XL-MIMO-OFDM systems using LSFD versus the distance between APs and rail track ($K = 4, N = 256, v = 300$ km/h).

where $\mathrm{SINR}_k^{\mathrm{c}}[s]$ *is given by*

$$p_k \left|\left(\mathbf{v}_k^{\mathrm{c}}[s]\right)^{\mathrm{H}} \mathbf{q}_k^{\mathrm{c}}[0]\right|^2 \left(p_k \sum_{m \neq s}^{M} \left|\left(\mathbf{v}_k^{\mathrm{c}}[s]\right)^{\mathrm{H}} \mathbf{q}_k^{\mathrm{c}}[m-s]\right|^2 + \sum_{i \neq k}^{K} p_i \sum_{m=1}^{M} \left|\left(\mathbf{v}_k^{\mathrm{c}}[s]\right)^{\mathrm{H}} \mathbf{q}_i^{\mathrm{c}}[m-s]\right|^2 + \left(\mathbf{v}_k^{\mathrm{c}}[s]\right)^{\mathrm{H}} \sigma^2 \mathbf{I}_{LN} \mathbf{v}_k^{\mathrm{c}}[s] \right)^{-1}, \tag{29}$$

where

$$\mathbf{q}_i^{\mathrm{c}}[m-s] = J_i[m-s]\mathbf{h}_i^{\mathrm{c}}. \tag{30}$$

Furthermore, utilizing the MMSE combining

$$\mathbf{v}_k^{\mathrm{c}}[s] = p_k \left(\sum_{i=1}^{K} p_i \sum_{m=1}^{M} \left(\mathbf{q}_i^{\mathrm{c}}[m-s] \left(\mathbf{q}_i^{\mathrm{c}}[m-s]\right)^{\mathrm{H}} \right) + \sigma^2 \mathbf{I}_{LN} \right)^{-1} \mathbf{q}_k^{\mathrm{c}}[0], \tag{31}$$

the highest value of (29) is referred to as $\mathrm{SINR}_k^{\mathrm{c,mmse}}[s]$ and can be calculated as

$$p_k \left(\mathbf{q}_k^{\mathrm{c}}[0]\right)^{\mathrm{H}} \left(p_k \sum_{m \neq s}^{M} \mathbf{q}_k^{\mathrm{c}}[m-s] \left(\mathbf{q}_k^{\mathrm{c}}[m-s]\right)^{\mathrm{H}} + \sum_{i \neq k}^{K} p_i \sum_{m=1}^{M} \mathbf{q}_i^{\mathrm{c}}[m-s] \left(\mathbf{q}_i^{\mathrm{c}}[m-s]\right)^{\mathrm{H}} + \sigma^2 \mathbf{I}_{LN} \right)^{-1} \mathbf{q}_k^{\mathrm{c}}[0]. \tag{32}$$

IV. Numerical Results

In this part, we aim to demonstrate the validity of our theoretical analysis through simulation results and exhibit the capabilities of XL-MIMO in high-speed contexts. A simulation setup is designed, in which L APs (ELAAs) are positioned along one side of a 1000 m railway, with uniform intervals between each AP (ELAA).

In Fig. 3, the performance of HST in XL-MIMO-OFDM systems using MMSE combining is compared to that of cellular and small cell systems with centralized and local processing. The results show that the centralized processing in the XL-MIMO-OFDM system provides nearly three times the gain in HST communications than the small cell system, thanks to the ability to calculate the ideal MMSE combining vector by using channel state information (CSI) from the entire network, reducing interference effectively. Local processing in the XL-MIMO-OFDM system, by utilizing LSFD cooperation, also shows a 59% SE performance improvement compared to the small cell system. However, the SE performance of HST varies greatly based on its position, due to phase-shift and large-scale fading. Fig. 3 (b) illustrates that XL-MIMO-OFDM systems with centralized and local processing offer high SE performance for HST communications.

In Fig. 4, the average SE is plotted against the distance between the APs and the railway for different numbers of APs. As the figure illustrates, SE initially rises rapidly and reaches a peak before gradually declining as the distance between the APs and the railway increases. There is a specific value of d_z that leads to the highest average SE. This behavior is due to the trade-off between the decrease in the DFO effect and the increase in path loss with increasing distance. Additionally, having a smaller number of APs increases the optimal value of d_z at which the maximum average SE is achieved.

Fig. 5 shows the average SE in XL-MIMO-OFDM systems using LSFD cooperation varies with different deployment modes and a fixed total number of antennas. When the total number of antennas per 1000 meters of the track is LN, it has been determined that the best way to distribute them is through a CF setup using LN APs with one antenna each. The reason for this is that having more APs allows for greater use of spatial degrees of freedom, providing better coverage and reducing the DFO effect by ensuring that there are always APs with small angles of arrival. However, more APs also require more fronthaul links, which increase the signal processing complexity. Thus, it is beneficial to use a lower number of antennas per AP to decrease the complexity of fronthaul links without greatly impacting performance.

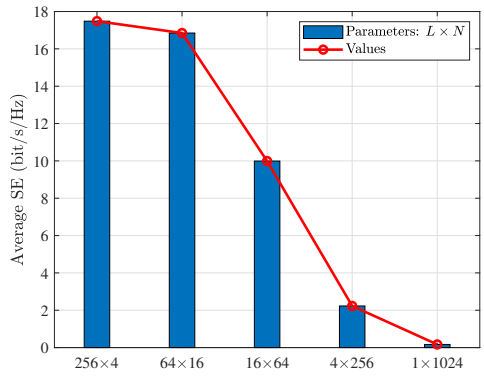

Fig. 5. Average SE using LSFD cooperation varies with different deployment modes ($L \times N = 1024, d_z = 50$ m, $v = 300$ km/h).

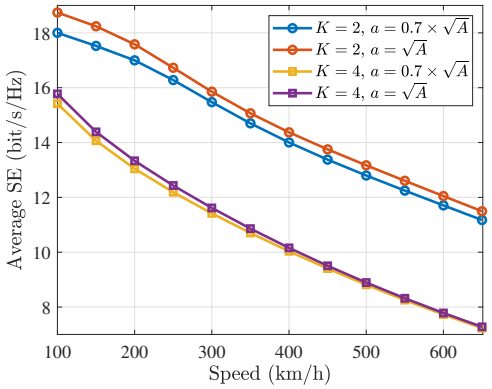

Fig. 6. Average SE varies with different numbers of TAs and the area of the antennas with fixed spacing ($K = 4, L = 10, N = 256, d_z = 50$ m).

Fig. 6 compares the average SE changing with different numbers of TAs and the size of the antennas while maintaining a fixed spacing. It is evident that the SE performance can be enhanced by increasing the area of the antennas and reducing the number of TAs. A smaller antenna area will result in a smaller SE, but this gap will gradually decrease as the speed increases. When the antenna area stays constant, the average SE of a smaller K decreases at a slower rate as speed increases. This is because as the speed increases, the DFO effect between TAs and APs will gradually increase and then dominate. At the same time, a smaller K and a smaller antenna area will reduce the effect of DFO.

V. Conclusion

In this paper, we examined the potential of XL-MIMO-OFDM systems for HST communications. More specifically, our focus was on examining the uplink SE in a moving LoS scenario and investigating the impact of large ICI caused by DFO. It is interesting to find that increasing the number of APs leads to a significant improvement in average SE, with a smaller distance between the APs and the railway being the optimal point for SE. Furthermore, an improvement in average SE can be achieved by increasing the number of APs and decreasing the number of antennas per AP, while keeping the total number of antennas constant. On the other hand, reducing the impact of DFO can be accomplished by shrinking the size of the antennas and decreasing the number of TAs in a fixed-size ELAA.

References

[1] J. Zhang, E. Björnson, M. Matthaiou, D. W. K. Ng, H. Yang, and D. J. Love, "Prospective multiple antenna technologies for beyond 5G," *IEEE J. Sel. Areas Commun.*, vol. 38, no. 8, pp. 1637–1660, Aug. 2020.

[2] G. Berardinelli, E. J. Khatib, R. Hashemi, C. de Lima, M. Latva-aho *et al.*, "A functional architecture for 6G special purpose industrial IoT networks," *arXiv:2207.00264*, 2022.

[3] E. Björnson, L. Sanguinetti, H. Wymeersch, J. Hoydis, and T. L. Marzetta, "Massive MIMO is a reality—what is next?: Five promising research directions for antenna arrays," *Digit. Signal Process.*, vol. 94, pp. 3–20, Jun. 2019.

[4] J. Zhang, H. Liu, Q. Wu, Y. Jin, Y. Chen, B. Ai, S. Jin, and T. J. Cui, "RIS-aided next-generation high-speed train communications: Challenges, solutions, and future directions," *IEEE Wireless Commun.*, vol. 28, no. 6, pp. 145–151, Dec. 2021.

[5] J. Zhang, H. Du, P. Zhang, J. Cheng, and L. Yang, "Performance analysis of 5G mobile relay systems for high-speed trains," *IEEE J. Sel. Areas Commun.*, vol. 38, no. 12, pp. 2760–2772, Dec. 2020.

[6] Y. Guo, J. Zhang, Z. Lu, and M. Wang, "Beam tracking and coverage enhancement algorithm for mobile users with intelligent reflecting surface," *ZTE Commun.*, vol. 27, no. 2, pp. 54–59, Apr. 2021.

[7] Y. Zhao, J. Zhang, and B. Ai, "Applications of reconfigurable intelligent surface in smart high speed train communications," *ZTE Commun.*, vol. 27, no. 4, pp. 36–43, Aug. 2021.

[8] R. He, B. Ai, G. Wang, K. Guan, Z. Zhong, A. F. Molisch, C. Briso-Rodriguez, and C. P. Oestges, "High-speed railway communications: From GSM-R to LTE-R," *IEEE Trans. Veh. Technol.*, vol. 11, no. 3, pp. 49–58, Sep. 2016.

[9] Z. Xiao, L. Zhu, and X.-G. Xia, "UAV communications with millimeter-wave beamforming: Potentials, scenarios, and challenges," *China Commun.*, vol. 17, no. 9, pp. 147–166, Sep. 2020.

[10] H. Lu and Y. Zeng, "Communicating with extremely large-scale array/surface: Unified modeling and performance analysis," *IEEE Trans. Wireless Commun.*, vol. 21, no. 6, pp. 4039–4053, Jun. 2021.

[11] J. Zheng, J. Zhang, E. Björnson, and B. Ai, "Impact of channel aging on cell-free massive MIMO over spatially correlated channels," *IEEE Trans. Wireless Commun.*, vol. 20, no. 10, pp. 6451–6466, Oct. 2021.

[12] W. Jiang and H. D. Schotten, "Cell-free massive MIMO-OFDM transmission over frequency-selective fading channels," *IEEE Wireless Commun. Lett.*, vol. 25, no. 8, pp. 2718–2722, Aug. 2021.

[13] P. Ramezani and E. Björnson, "Near-field beamforming and multiplexing using extremely large aperture arrays," *arXiv:2209.03082*, 2022.

[14] J. Zheng, J. Zhang, E. Björnson, Z. Li, and B. Ai, "Cell-free massive MIMO-OFDM for high-speed train communications," *IEEE J. Sel. Areas Commun.*, vol. 40, no. 10, pp. 2823–2839, Oct. 2022.

[15] J. Zhang, J. Zhang, D. W. K. Ng, and B. Ai, "Federated learning-based cell-free massive MIMO system for privacy-preserving," *IEEE Trans. Wireless Commun.*, Dec. 2022.

[16] J. Zhang, J. Zhang, D. W. K. Ng, S. Jin, and B. Ai, "Improving sum-rate of cell-free massive MIMO with expanded compute-and-forward," *IEEE Trans. Signal Process.*, vol. 70, pp. 202–215, Nov. 2021.

[17] J. Zhang, J. Zhang, E. Björnson, and B. Ai, "Local partial zero-forcing combining for cell-free massive MIMO systems," *IEEE Trans. Commun.*, vol. 69, no. 12, pp. 8459–8473, Dec. 2021.

[18] E. Björnson, J. Hoydis, L. Sanguinetti *et al.*, "Massive MIMO networks: Spectral, energy, and hardware efficiency," *Foundations and Trends® in Signal Processing*, vol. 11, no. 3-4, pp. 154–655, Nov. 2017.

[19] J. Zheng, J. Zhang, E. Björnson, and B. Ai, "Impact of channel aging on cell-free massive MIMO over spatially correlated channels," *IEEE Trans. Wireless Commun.*, vol. 20, no. 10, pp. 6451–6466, Oct. 2021.

[20] J. Zheng, J. Zhang, and B. Ai, "UAV communications with WPT-aided cell-free massive MIMO systems," *IEEE J. Sel. Areas Commun.*, vol. 39, no. 10, pp. 3114–3128, Oct. 2021.